Analysis of $B^0 \to K^+ \pi^- e^+ e^-$

Master Thesis

Ana Roldán

aroldan@student.ethz.ch

Experimental Flavour Physics Group
Physik Institute, University of Zurich
Department of Physics
ETH Zürich

Supervisors:
Prof. Dr. Nicola Serra, Dr. Patrick Owen
Prof. Dr. Günther Dissertori

December 22, 2022

Abstract

In the Standard Model (SM) of particle physics, the electroweak coupling of leptons to gauge bosons is independent of their flavour, thus the model is referred to as exhibiting lepton universality (LU). Recently, slight deviations from this behaviour have been observed. One of these deviations corresponds to the measurement of the $R_{K\pi}$ ratio between the branching fractions of the rare decay $B^0 \to (K^{*0} \to K^+\pi^-)l^+l^-$, of the $l = e$ electron and the $l = \mu$, muon channels. This deviation was measured at the Large Hadron Collider (LHC) in the region of the invariant mass $m(K^+\pi^-)$ between $792 < m(K^+\pi^-) < 992$ MeV/c^2, and in the dilepton mass-squared (q^2)range between $1.1 < q^2 < 6.0$ GeV/$^2c^4$. Thus, further exploration of the behaviour of the $R_{K\pi}$ ratio in other regions of $m(K\pi)$ is essential. For such an analysis, a series of pre-selections and cuts have to be applied to the data collected at the LHC, in order isolate the signal from the background. However there are some backgrounds that cannot be successfully eliminated by the application of these cuts, specifically in the case of $B^0 \to K^+\pi^-e^+e^-$, due to the nature of electrons. In this thesis, we use RapidSim to generate some of these irreducible backgrounds and study their effect and bias on the signal $B^0 \to K^+\pi^-e^+e^-$ in the invariant mass window $992 < m(K\pi) < 2600$ MeV/c^2, for the dilepton mass squared window of the electron-positron pair $1.1 < q^2 < 7.0$ GeV/$^2c^4$.

Acknowledgements

I would like to take this opportunity to thank everyone that supported me and helped me in the completion of this project, specially given the current circumstances of my health.

First, I want to thank Prof. Dr. Nicola Serra for giving me the opportunity to write my thesis with his research group at the University of Zurich. I would also like to thank Dr. Patrick Owen, for his patience, support and for all the discussions we have had during the past year. Similarly I want to thank Prof. Dr. Gunther Dissertori for kindly agreeing to be my supervisor.

I am very grateful to all the members of the LHCb Flavour Physics group at UZH for all the talks and help they shared with me during this process. It was truly a pleasure to share a workspace with all of them.

Furthermore I would like to thank all the people who have helped in the process of my recovery, specially to my dearest Johannes and Sam, and my doctors Hanna and Lina.

Contents

List of Figures

List of Tables

Introduction

The Standard Model (SM) of Particle Physics is one of the most successful theories ever developed. Despite the fact that predictions derived from this model are in good agreement with experimental results, it still leaves several fundamental questions unanswered. Among them are the mystery of the flavour structure of matter, the arrangement of fermions in three families and the universality of the couplings among their interactions.

Multiple new physics (NP) models try to explain these enigmas by suggesting the existence of new types of particles, that would underlyingly give rise to the arrangements in the structure of matter we currently observe. Such models predict deviations from the expected SM behaviour of certain sub-atomic processes, as it is the case of lepton universality (LU).

A well suited channel to probe the effects of NP on lepton universality is the rare decay $B^0 \to K^+\pi^- l^+ l^-$, where B^0 is a neutral B meson, K^+ and π^- are a charged kaon and pion respectively, and l is either a muon μ or an electron e. LU can be tested through the analysis of the ratio of the branching fractions between the e and μ channels of this decay, by using data collected in particle accelerators.[2]

The Large Hadron Collider (LHC), the largest and most powerful particle accelerator ever built, aims to help shed light on the reasons behind the fundamental structure of matter by testing the limits of the SM and searching for hints of NP. The LHCb, one of the four LHC big experiments, searches for NP by measuring decays involving B mesons produced in proton-proton collisions at the LHC. Data collected at this experiments is particularly well suited to study decays such as $B^0 \to K^+\pi^- l^+ l^-$.

Given that thousands of different B mesons decays are detected at the LHCb every second, large statistical samples are collected. Thus, a fundamental part of any type of analysis of this data, involves the isolation of the specific channel containing the signal to be studied. This is achieved in part by a sophisticated system of triggers built-in the experiment itself, and in part by applying a series of selections and cuts to the acquired data to try to eliminate all the non wanted events, the background, while aiming to preserve as many signal events as possible. This is an onerous task, especially for B meson decays involving electrons, due to Bremsstrahlung effects that affect their detection.

This thesis provides a framework to understand the contaminating effect of a subset of decays of the rare B meson channel $B^0 \to K^+\pi^- e^+ e^-$ in the invariant

mass region $992 < m(K\pi) < 2600$ MeV/c^2 with a dilepton mass-squared of the electrons-positron pair in the range $1.1 < q^2 < 7.0$ GeV/c^2.

Chapter 1 lays the foundation of the relation between the SM and the flavour structure of matter. Chapter 2 briefly explain the LHCb experiment and expands on previous measurements that hint at deviations of LU. Chapter 3 contains the bulk of the analysis conducted, explaining the tools used to simulate the signal, the interest in the the specific invariant mass region selection applied, and the type of decays that are prone to contaminate the signal in this region. The thesis is closed by a summary of the observed effects that the backgrounds have on the signal by commenting on efficiency of the mass vetoes applied and the resulting parameters of the fitting analysis performed.

Chapter 1

The Standard Model of Particle Physics

1.1 Overview

The SM of particle physics provides a robust framework for the interactions of the smallest constituents of matter. It successfully explains most of the observed phenomena in elementary particle physics encompassing the strong, electromagnetic (EM) and weak interactions. The elementary particles that form the SM can be split in two groups: fermions and boson.

Fermions, known as matter fields, are classified in quarks and leptons depending on their spin. Quarks are the building blocks of all hadrons[1], they are endowed with color and electro-weak charges. Leptons do not have color charges but only electro-weak charges.

Matter fermions come in three generations or families with identical quantum numbers but different masses. Each family contains a weakly charged doublet of quarks $(+2/3, -1/3)$, in three color replicas; and a colorless weakly charged doublet with a neutrino and a corresponding charged lepton. There is currently no explanation for this triple repetition of fermion families.

Bosons, known as force carriers are classified based on the type of interaction that they mediate. The EM interaction is mediated by the photon γ, the weak interaction by the gauge bosons W^+, W^- and Z^0 and the the strong interaction by a total of eight different bosons known as gluons g.

The photon and the gluons have zero masses as a consequence of the exact conservation of its corresponding symmetry generators, the electric charge and the eight color charges.

The weak bosons on the other hand have large masses as a consequence of the breaking of their corresponding symmetry induced by the Higgs mechanism.

[1] Hadrons are composite subatomic particles made of two or more quarks held together by the strong interaction.

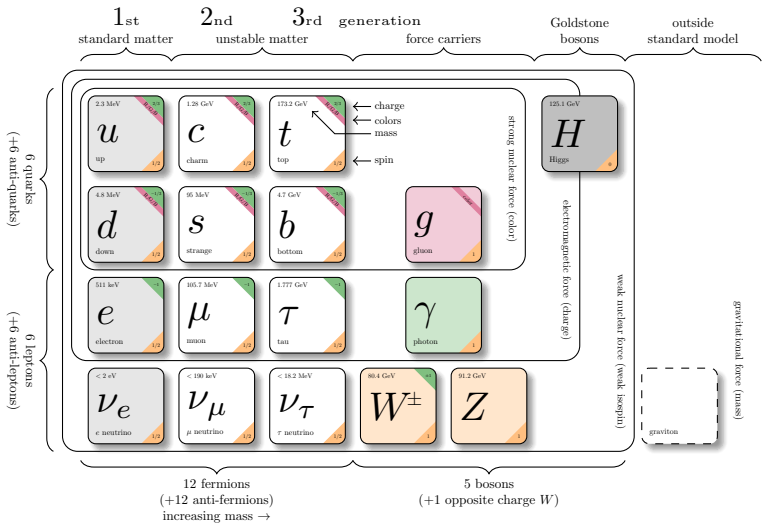

Figure 1.1: Summary of the properties of all particles described by the Standard Model.[2] The corresponding charges, families and interactions are indicated for each of them.[1]

A total of 17 fundamental particles and their corresponding anti-particles are described by the SM. Figure 1.1 outlines this classification. To understand the behaviour and interaction between all SM particles, we need to have a look at its underlying mathematical structure.

1.2 Gauge Structure of the Standard Model

The SM is a generalisation of Quantum Electrodynamics (QED), as it is a renormalizable field theory based on a local symmetry (i.e. a field theory that is separately valid at each point in space-time, thus it is independent of the energy scale) that extends the gauge invariance of electrodynamics to a larger set of conserved currents and charges.[6]

In the SM there are eight strong charges associated to gluons, called "color" charges; and four electroweak (EW) charges (where the the electric charge is included) associated to the weak and electromagnetic bosons.

The quantum chromodynamics (QCD) sector which defines the interactions between quarks and gluons, is a Yang–Mills gauge theory with $SU(3)$ symmetry. While the EW sector is a Yang–Mills gauge theory with the symmetry group $SU(2)_L \bigotimes U(1)$.[6]

[2] A graviton is a hypothetical particle representing the interaction of matter with gravity.

The commutators of the strong and electroweak charges form a symmetry group. Thus, the SM can be mathematically described as a gauge theory based on the symmetry group $SU(3) \bigotimes SU(2)_L \bigotimes U(1)_Y$. However, the non vanishing expectation value of the Higgs field breaks this symmetry and reduces it to $SU(3)_C \bigotimes U(1)_{EM}$.

The spontaneous symmetry breaking (SSB) of the gauge symmetry associated with the EW interaction, $SU(2)_L \bigotimes U(1)_Y$, generates masses for several particles, and separates the electromagnetic and weak forces.

The Higgs mechanism does not affect the universality of the gauge couplings. Thus in the SM, all three fermion families have the same gauge charges leading to the same coupling structures.

The differences in mass between the three families come exclusively from the interaction between the Higgs fields and the fermion fields. This interaction is known as the Yukawa interaction and is what grant fermions their mass.

The Yukawa coupling breaks the flavor symmetry as it couples differently to each of the three fermion families. This results in the three otherwise identical families of fermions, that only differ in mass.

This coupling difference, caused by the SSB of the EW interaction, has another effect. It also results in the mixing between the electroweak eigenstates and the mass eigenstates.[3] This mixing occurs during the coupling of fermions to the W boson. This is the origin of flavor changing nature that weak charged currents (i.e. couplings involving the $W^{\pm}$ boson) have on fermions.

This is why interactions involving photons (γ), gluons or Z^0 bosons do not change the flavor of the participating quarks (i.e. transform one quark type into another), but interactions mediated by a charged gauge boson $W^{\pm}$ do.

As a consequence of the Higgs mechanism being the only source of difference between the 3 generations of particles,[7] the electroweak coupling of leptons to gauge bosons in the SM is independent of their flavour, and the flavor changing nature of fermions is mediated exclusively by the $W^{\pm}$ boson.

1.3 Lepton Universality

As seen in the previous sections, the three generations of lepton doublets are identical to each other, except for their mass. As well, the electroweak couplings of leptons to gauge bosons are independent of their respective flavour. Hence, leptonic decays involving the electroweak interaction should have equal branching

[3] Given that Yukawa matrix cannot be diagonalized simultaneously in mass and flavor eigenstates

fractions with all the three different families.[4] This is referred to as the SM exhibiting *Lepton Flavor Universality*.

Lepton universality is an 'accidental' symmetry of the SM. It is called 'accidental' because the SM Yukawa couplings arise at the renormalizable level, (i.e. they are not imposed by a symmetry group, they simply appear at low energy levels). In other words, these couplings are free parameters of the Standard Model.

This is one of several unexplained phenomena left unexplained by the SM. Some of these puzzling phenomena are thought be a consequence of the global remnant of some spontaneously broken gauge symmetry. Which is why several NP models propose the extension of the fermion content of the SM such as to encompass yet another symmetry group. Aiming to account for its previously mentioned limitations.

Within this framework of extensions of the SM one generically expects flavor non-universality to emerge in charged leptons at high energies, in such a way that it would naturally prevent lepton flavor violation, by aligning the mass and weak eigenbases.[8]

NP particles theorised to exist include leptoquarks and new types of gauge bosons. Both such as to mediate new unforeseen interactions between leptons and quarks.

1.4 Flavour Changing Weak Currents

As discussed previously, due to the mixing of weak and mass eigenstates occurring when fermions couple to W bosons, fermions are only able to change flavor through a weakly charged interaction.

This means that by the emitting a W boson, an up-type quark ($u-$quark) can be turned into a down-type quark ($d-$quark). Flavor changes do not only occur within the same generation (e.g. $d \to W^- u$), but also across generations (e.g. $b \to W^- u$).

The amplitude of a changing flavor interaction from a $i-$quark to a $j-$quark, $i \to Wj$, where $i, j = (u, d, c, s, t, b)$, is proportional to the corresponding element $|V_{ij}|$ of the Cabibbo-Kobayashi-Maskawa matrix (V_{CKM}).

$$|V_{CKM}| = \begin{pmatrix} |V_{ud}| & |V_{us}| & |V_{ub}| \\ |V_{cd}| & |V_{cs}| & |V_{cb}| \\ |V_{td}| & |V_{ts}| & |V_{tb}| \end{pmatrix} \approx \begin{pmatrix} 0.974 & 0.225 & 0.003 \\ 0.225 & 0.973 & 0.041 \\ 0.009 & 0.004 & 0.999 \end{pmatrix} \tag{1.1}$$

[4] The Branching fractions between the three families are predicted to be identical by the SM, aside from phase space differences.

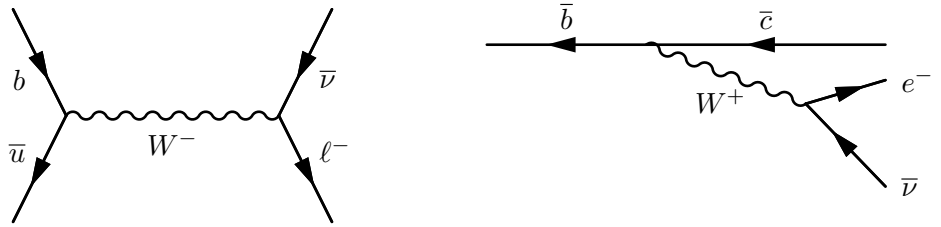

Figure 1.2: On the left, a diagram showing flavor change through an annihilation process. On the right, the flavor changing part of a simple spectator diagram is shown.

Since the V_{CKM} quark mixing matrix is found to be approximately diagonal, processes involving transitions across families are suppressed. This is known as **Cabbibo suppression**.[9]

For instance, a transition between $b \to W^- u$ is consider suppressed, as its amplitude is proportional to $|V_{ub}| \approx 0.003$. The smaller the value of the amplitude, the rarest the process.

The exact calculation of probability amplitudes of a specific transition requires the use of rather large and complicated integrals over a large number of variables. Feynman diagrams are visual representations of these.[6] Thus, a pictorial representation of the amplitude of a transition can be deduced by the nature of its respective Feynman diagram.

Weak charged currents are the only tree level interactions in the SM that can change the flavor of a fermion, see diagrams in figure 1.2. In these examples, we can see that by changing the flavor through the emission or absorption of $\mathrm{W}^{\pm}$ boson, by the charged nature of the boson, the resulting quarks have a different electric charge that the initial ones. For instance, in the transition $\overline{b} \to \overline{c}$, the initial $\overline{b}-$quark has an electric charge of $+1/3$ and the resulting $\overline{c}-$quark, a charge of $-2/3$.

It is also possible to change the flavor of a quark without altering the electric charge between the initial and final states. This process is known as a **flavour changing neutral current** (FCNC).

An example of a FCNC process would be a transition where a $b-$quark is changed into an $s-$quark, here the flavor has changed, but both the initial and final state charge is $-1/3$. Thus, this interaction has not altered the electric charge of the fermion, only its flavor.

A FCNC transition from $b \to s$ would require the contribution of electroweak loop Feynman diagram. Diagrams in figure 1.3 are examples of such processes.

Such transition would require first to change the flavor of the initial $b-$quark to a u-quark (or c, $t-$quark), and then to change the flavor of the u-quark to an $s-$quark. The amplitude of such transition would be proportional to $|V_{us}| \cdot |V_{ub}|$.

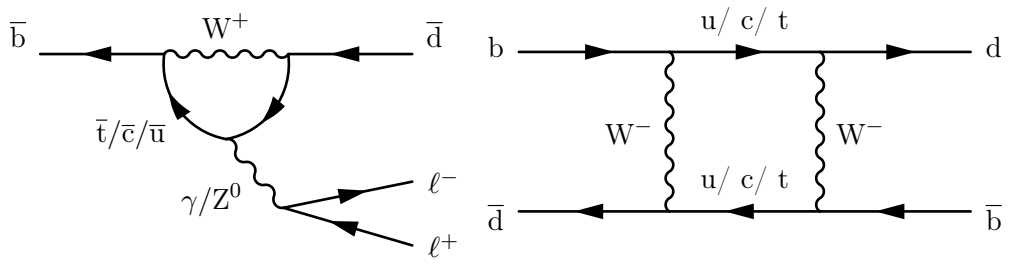

Figure 1.3: Loop Feynman diagrams representing FCNC processes. On the left, the penguin diagram and on the right, the box diagram. In both cases the flavor of the initial and final state quarks is different, although the electric charge remains unchanged.

The fact that FCNC decays allow only for the contribution of electroweak loop Feynman diagrams, together with the suppression of transitions across families due to the diagonal nature of the Cabbibo matrix, results in FCNC being forbidden at tree level in the framework of the SM.

This is what makes these types of transitions a good probe for NP. It is expected that the presence of NP particles would result in additional NP diagrams, diagram that will make **observable** contributions to the decay modes of such processes. This type of contributions can be seen in the diagrams shown in figure 1.5 representing the $\overline{b} \to \overline{s}$ transition.

1.5 B meson Decays

B mesons are bound states of a $b-$quark and a light anti-quark. The bound states containing a b quark and a $\overline{u}$, $\overline{d}$ or $\overline{s}$ anti-quark are referred to as $B_d(B^0)$, $B_u(B^-)$ and B_s mesons, respectively.[10]

While the binding between the $b-$quark and the light anti-quark is provided by the strong interaction[5], B mesons can only decay via the weak interaction.[11] which accounts for their relatively long life times, $\approx 10^{-2}$s.

An interesting aspect of these mesons is the fact that the $b-$quark is not allowed to decay within his own family due to cabbibo suppression and the nature of its quark doublet, the $t-$quark.

B meson decays occur primarily through via the $b \to W^- c$ transition, with this decay channel being proportional to $V_{cb} \approx 0.41$ component of the V_{CKM} matrix. In such decays the corresponding dominant weak decay Feynman diagram

[5]In nature quarks are subject to color confinement. The strong interaction binds quarks together in clusters to form colorless hadrons.

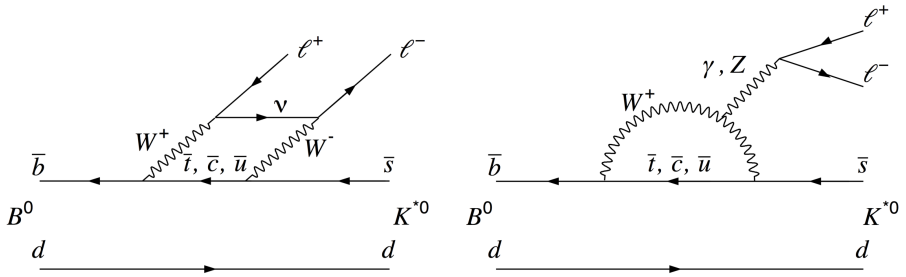

Figure 1.4: Feynman diagrams of the $B_0 \to K^{*0} l^+ l^-$ decay. On the left a type of interaction known as the penguin diagram and on the right, the box diagram.[2]

is the spectator diagram shown in figure 1.2. All B meson decays that do not occur through the usual $b \to c$ transition are known as *rare B decays*.

As explained in the previous section, B mesons can also decay via FCNC processes, such like transitions of the type $b \to s$ and $b \to c$. An interesting example involving such transition is the decay $B^0 \to K^{*0} l^+ l^-$.

Due to the K^{*0} being compose of a $d-$quark and an $\bar{s}-$antiquark, this process can be represented through the one-loop flavor-changing neutral current diagram, also known as the "penguin" diagram, see figure 1.4. The V_{CKM} favoured part of this diagram, corresponding to a $\bar{b} \to \bar{s}$ transition, is expected to dominate the amplitude of rare decays to final states with one or three $s-$quarks.

A transition involving $b \to c$ is also possible, however is highly suppressed by the components of the V_{CKM} matrix, as it would be proportional to the $|V_{cd}| \approx 0.225$ term instead of the much larger $|V_{cs}| \approx 0.973$ term.

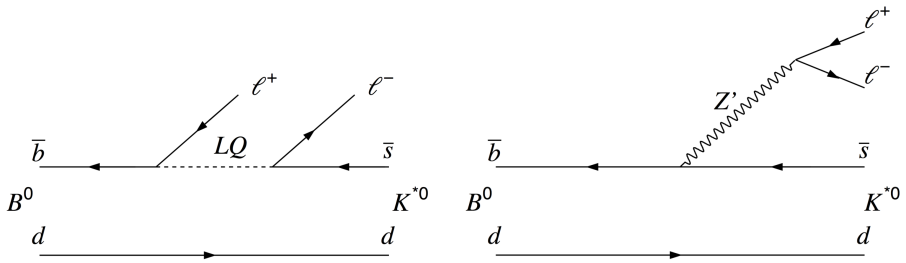

Figure 1.5: Diagrams of possible NP contributions that would violate LU such as a tree level diagram mediated by a new gauge boson Z' on the left, and a tree level diagram involving a leptoquark LQ on the right.[2]

All of the above, make FCNC loop level decays of the type $b \to s l^+ l^-$ an excellent probe for NP. The presence of any NP particles could lead to a sizeable increase or decrease in the rate of processes involving this transition, or change the angular distribution of the final state particles. Furthermore this type of decay, by the presence of a lepton anti-lepton pair in its final state, offers a

robust test of the effects of NP on lepton universality.

Given all of this, it is not surprising that current studies of NP are focused on the analysis of decays of this type, specially relying on the amount of data provided by experiments like the LHCb.[12]

1.6 Hints of LU Violation

In recent years several hints of LU violations have been detected. For instance evidence of the breaking of lepton universality in beauty-quark decays, with a significance of 3.1 standard deviations, based on proton–proton collision has been collected with the LHCb detector at LHC.[13]

Even if the observed pattern of deviations from the SM predictions may hint at the existence of new physics. None of these deviations was statistically significant enough to constitute clear signs of new physics on their own, mainly because the large uncertainty on the correct detection and identification of electrons.

However, one of the most interesting results comes from the analysis of the $B^0 \to K^{*0} l^+ l^-$ process, as small discrepancies have been detected while measuring the ratio of the branching fractions of the $B^0 \to K^{*0} \mu^+ \mu^-$ and $B^0 \to K^{*0} e^+ e^-$ are the most precise to date.

As explained in the previous section, this process would be very sensitive to the effects of NP, and by extension to the presence of NP particles that if real, could be the source of the LU violations detected. Possible scenarios for this argument include the existence of a lepto quark LQ type of particle or a new gauge boson Z', in both cases these particles would affect the production of electron-positron pairs and muon-antimuon pairs differently, as they would couple to the three families in a different way. This could provide further insight on the until now unexplained flavour structure of matter. The possible Feynman diagrams for these hypothetical NP process are presented in figure 1.4.

Chapter 2

The LHCb Experiment

2.1 The LHC

The Large Hadron Collider (LHC) is a hadron accelerator and collider aimed to the search of physics beyond the standard model (BSM), through various direct and indirect experiments. In its main operation mode, the LHC collide protons with each other at center-of-mass energies up to 14 TeV. Protons are accelerated and brought to collision at four crossing points points in bunches, with a nominal bunch spacing of 25 ns, corresponding to a frequency of 40 MHz.

Around every one of the four collision points, there are several experiments, each designed to detect different phenomena. The four largest experiments are ATLAS, CMS, ALICE and LHCb, but there are other smaller more specialzed ones such like TOTEM, MoEDAL, LHCf, SND and FASER as well.

If we were to record all the interactions produced at the LHC, we would collect a petabyte (PB) of data every single second. However, not all the interactions produced are of interest to every experiment. For this reason each experiment is build with a series of sophisticated trigger systems to record mostly the events they are dedicated to studying.

Even with such a built-in pre-selection, the amount of data collected by the experiments amounts to 15 PB per year. This is why a bast amount of computing power, and a collaboration of scientist from all around the world, are needed to process this data and extract results. This thesis is dedicated to provide some insight into future data analysis of one of this processes.

2.2 The LHCb Detector

As mention above, the LHCb experiment is one of the four large experiments at the LHC. Its focused on studying charge parity (CP) violating processes in B physics as well as rare decays of B mesons. In section 1.5 we discussed the interest on these type of decays.

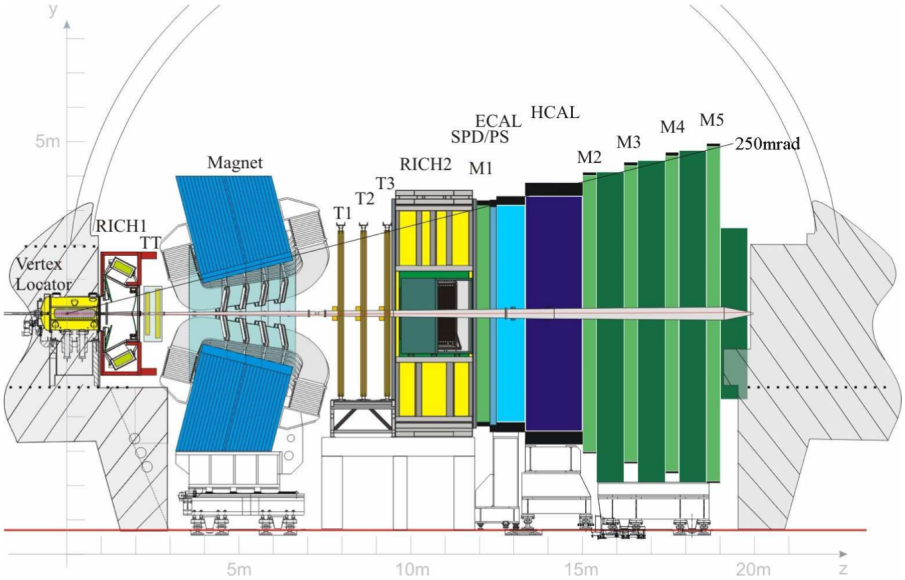

Figure 2.1: View of the LHCb detector along the bending plane.[3]

The LHCb detector is designed as a single-arm forward spectrometer with an acceptance in terms of pseudorapidity[1] of $\eta = 1.9 - 5.3$. The choice of the detector geometry is justified by the fact that at high energies both the $b-$ and $\bar{b}$-hadrons are predominantly produced in the same forward or backward cone (i.e. under low angles) with respect to the beam of the hadron collider.

The detector includes a high-precision tracking system consisting of a silicon-strip vertex detector surrounding the proton-proton interaction region, a large-area silicon-strip detector located upstream of a dipole magnet with a bending power of about 4 terameters (Tm), and three stations of silicon-strip detectors and straw drift tubes placed downstream of the magnet. The detector set-up is shown in figure 2.1.

The tracking system provides a measurement of momentum $\overrightarrow{p}$, with a relative uncertainty that varies from 0.5% at low values to 1.0% at 200 GeV/c. The minimum distance of a track to a primary vertex (PV), the impact parameter (IP), is measured with a resolution of $(15+29/p_T)\mu m$, where p_T is the component of the momentum transverse to the beam, in GeV/c. Different types of charged hadrons are distinguished using information from two ring-imaging Cherenkov detectors. Photons, electrons and hadrons are identified by a calorimeter system consisting of scintillating-pad and preshower detectors, an electromagnetic calorimeter (ECAL) and a hadronic calorimeter (HCAL). Muons are identified

[1] Pseudorapidity is a spatial coordinate that describes the angle of a particle relative to the beam axis

by a system composed of alternating layers of iron and multiwire proportional chambers.[3]

The trigger system consists of a hardware stage, based on information from the calorimeter and muon systems, followed by a software stage, which applies a full event reconstruction. The hardware muon trigger selects events containing at least one muon with significant p_T (from $\sim$ 1.5 to $\sim$ 1.8 GeV/c, depending on the data-taking period). The hardware electron trigger requires the presence of a cluster of calorimeter cells with significant transverse energy (E_T), (from $\sim$ 2.5 to $\sim$ 3.0 GeV, also depending on the data-taking period) in the ECAL. The hardware hadron trigger requires the presence of an energy deposit with E_T above $\sim$ 3.5 GeV in the calorimeters. The software trigger requires a $two-$, $three-$ or $four-$track secondary vertex, with a significant displacement from the PV. At least one charged particle must have significant p_T and be inconsistent with originating from any PV.[3] For the identification of secondary vertices consistent with $b-$hadron decays a multivariate algorithm is used.[2]

LHCb was originaly designed to study the decay of beauty and charm hadrons, although as of 2022, a series of new hadrons have been discovered by the LHCb collaboration, together with the apparent existence of pentaquarks.

2.3 Probes on Lepton Universality

As mentioned above, the LHCb experiment was built specifically to study rare B meson decays. Due to the nature of these type of decays their study can shed light into the limitations of the SM and the mysteries behind the flavor structure of matter.

Section 1.6 explained how the $B^0 \to K^{*0} l^+ l^-$ process has been of especial interest in the past, as this process can be used as particularly sensitive probe to test the limits of LU.[14] For this LU test, the observable of choice is the branching ratio between the branching fractions of the $B^0 \to K^{*0}\mu^+\mu^-$ and $B^0 \to K^{*0} e^+ e^-$ as defined by:

$$R_{K^{*0}} = \frac{\int_{q^2_{min}}^{q^2_{max}} \frac{d\Gamma(B^0 \to K^{*0}\mu^+\mu^-)}{dq^2}\, dq^2}{\int_{q^2_{min}}^{q^2_{max}} \frac{d\Gamma(B^0 \to K^{*0} e^+ e^-)}{dq^2}\, dq^2}$$

In this equation, the decay rate Γ, is integrated over a range of the squared dilepton invariant mass q^2. The advantage of selecting this observable, is that this ratio is precisely calculable in the SM framework due to large cancellations of hadronic uncertainties, and when integrated over all q^2 is predicted to yield $\mathrm{R}_{K\pi} = 1.0000 \pm 0.0001$. Thus offering a very precise test of LU.[15]

The K^{*0} represents the $K^*(892)^0$ meson that decays quickly through $K^*(892)^0 \to K^+\pi^-$. The resonance is reconstructed from the detection of the $K^+\pi$ final state by the LHCb. This is achieve by selecting candidates within 100 MeV/c^2 of the known mass of the $K^*(892)^0$, so the invariant mass of $K\pi$ was studied in the range $792 < m(K\pi) < 992$ MeV/c^2. In 2017, this ratio has been measured in two regions of q^2 as:

$$R_{K^{*0}} = \begin{cases} 0.66\ ^{+0.11}_{-0.07}\ \text{(stat)}\ \pm 0.03\ \text{(syst)} & \text{for} \quad 0.0045 < q^2 < 1.1\ \text{GeV}^2/\text{c}^4 \\ 0.69\ ^{+0.11}_{-0.07}\ \text{(stat)}\ \pm 0.05\ \text{(syst)} & \text{for} \quad 1.1 < q^2 < 6.0\ \text{GeV}^2/c^4 \end{cases}$$

With a corresponding 95.4% confidence level intervals of $\left[0.52, 0.89\right]$ and $\left[0.53, 0.94\right]$ respectively. This results are compatible with the SM expectations at the level of 2.1-2.3 and 2.4-2.5 standard deviations in the two q^2 regions, respectively.[2]

Nonetheless these measurements raise questions about the extend of the deviation from unity of this ratio in other regions of the invariant m($K\pi$).

Further exploration of this ratio in the invariant mass region $992 < m(K\pi) < 2600$ MeV/c^2 could offer corroboration of LU violation, or could discard it completely. Either way a thorough analysis of the behaviour of this ratio on this explored region would shed light in our current understanding of the structure of matter.

This is part of the motivation of the work presented in this thesis. As large part of the uncertainty contributions to the measurements of the $R_{K^{*0}}$ come from looseness in the electron identification criteria.

2.4 $B^0 \to K^+\pi^- l^+ l^-$

To explore the invariant mass region $992 < m(K\pi) < 2600$ MeV/c^2, instead of focusing on reconstructing the resonance K^{*0}, one can focus on the decay $B^0 \to K^+\pi^- l^+ l^-$. As before, the branching ratio between the branching fractions of the $B^0 \to K^+\pi^-\mu^+\mu^-$ and $B^0 \to K^+\pi^- e^+ e^-$ is defined as:

$$R_{K\pi} = \frac{\displaystyle\int_{q^2_{min}}^{q^2_{max}} \frac{d\Gamma(B^0 \to K^+\pi^-\mu^+\mu^-)}{dq^2}\, dq^2}{\displaystyle\int_{q^2_{min}}^{q^2_{max}} \frac{d\Gamma(B^0 \to K^+\pi^- e^+ e^-)}{dq^2}\, dq^2} \tag{2.1}$$

To produce a comparable result with the previous measurement, the q^2 is restricted to $1.1 < q^2 < 7.0$ GeV$^2/c^4$. A similar selection process and signal

treatment can be applied to the remaining unexplored invariant mass region of $K\pi$.

2.5 Selection Process

The data studied in the measurement of the $R_{K^{*0}}$ ratio was collected at LHCb during 2016 at a center-of-mass energy of 13 TeV with an integrated luminosity of 1.6 fb^1. The same dataset would be available in the analysis of the $R_{K\pi}$ ratio and similar selection process can be used with the isolation of the signals $B^0 \to K^+\pi^-\mu^+\mu^-$ and $B^0 \to K^+\pi^-e^+e^-$.

Such a selection process can help get rid of possible particle missidentification (missID) as well as exclude an array of similar backgrounds that would otherwise contaminate the signal region. However a possible source of contamination would be the presence of certain **irreducible backgrounds** than cannot be otherwise vetoed by the previously applied selection.

This type of irreducible backgrounds could have a large contaminating effect specially in the case of $B^0 \to K^+\pi^-e^+e^-$, due to the current challenges with the reconstruction of electrons.

2.6 Electron Reconstruction Effects

The experimental environment in which the LHCb detector operates leads to significant differences in the treatment of decays involving muons or electrons in the final state. The two types of leptons behave differently when travelling through the detector material.[3]

At the LHCb the trajectories of stable charged particles (tracks) need to be reconstructed accurately and with a high and well-known efficiency. The precise knowledge of this charged-particle reconstruction efficiency is essential in measurements of branching fractions.[16]

While muons are nearly unhindered by the LHCb detector material, electrons suffer from energy loss via bremsstrahlung. In some cases, the energy loss affects the trajectory to such a degree that the electrons no longer traverse all tracking detectors. If the larger amount of bremsstrahlung emitted by electrons is not properly accounted for, it would result in a significant degradation of the momentum resolution and consequently in a degradation of the B mass resolution. [16]

Due to the degradation on the momentum resolution of electrons, electron-hadron missidentification heavily affects the modeling of the residual misidentified hadronic backgrounds;

For B meson decays, these natural limitations degrade the resolution of the reconstructed invariant masses of both the dielectron pair and the B candidate. In decays with electrons, since the mass resolution of the reconstructed B candidate is worse than in final states with muons, the background contamination in the signal region is larger.

The level of combinatorial background, arising from the accidental association of particles produced by other $b-$ and $c-$hadron decays, is also higher in such channels, due to a larger number of electron candidates. As a result, the discriminating power of the fits to extract the signal yields is reduced significantly in the case of electrons.

This is the motivation behind discriminating most possible sources of contamination when treating a signal that has electrons in their final state, such as $B^0 \to K^+\pi^-e^+e^-$. Aiming to supply future analysis with tentative information about the contamination resulting from electron hadron missidentification, in this thesis we provide a preliminary analysis of such contamination using Monte Carlo (MC) simulated data of the signal and of a set of possible missID hadronic backgrounds.

Chapter 3

Data Analysis

The following analysis focus on gauging the possible effects that a set of irreducible backgrounds would have on the biasing of the signal $B^0 \to K^+\pi^-e^+e^-$.

A fast MC generator for simulation of heavy-quark hadron decays (RapidSim) is used to generate the signal and a subset of irreducible background that would appear in the same $m(K\pi)$ region where future analysis of the $R_{K\pi}$ could be focused.

This thesis aims to provide a baseline on the understanding of the contaminating effects of these irreducible hadronic backgrounds, as well as an understanding of the extend of the capabilities of the fast MC signal generator RapidSim.

3.1 RapidSim

RapidSim is a lightweight application for the fast simulation of phase space decays of beauty and charm quark hadrons, allowing for quick studies of the properties of signal and background decays in particle physics analyses.

It is build using the TGenPhaseSpace[1] class from the ROOT application, using externally provided fixed-order next-to-leading-logarithm calculations to boost the initial beauty and charm hadrons to the appropriate energy for the production environment of interest.[17]

To give the $b-$ and $c-$hadrons the correct production kinematics for the LHC it relies on FONLL[2].

User-defined momentum resolution functions can be used to mimic the effect of imperfect track reconstruction. Thus while generating the decays, it is possible

[1] TGenPhaseSpace is utility class capable to generate n-body events with constant cross-section or with Fermi energy dependence

[2] FONLL is parogram to calculate heavy quark transverse momentum and rapidity distributions in hadron-hadron and photon-hadron collisions, matching Fixed Order next-to-leading order terms and Next-to-Leading-Log large-p_T resummation.

for example to set the smear of the momenta of the daughter particles accordingly to their type.

User-defined efficiency shapes can be applied during generation to reproduce the effects of geometric and kinematic requirements on final state particles as well as the dynamics of the decay. Thus allowing for different sets of cuts to be applied to the properties of the daughter particles.

The effect of missidentification of the final state particles can be done via configuration files, while the framework can easily be extended to include additional particle types. Thus allowing for the swap of different particle mass hypothesis.

In this thesis, RapidSim was used to generate the $B^0 \to K^+\pi^-e^+e^-$ signal and a list of irreducible decays that can be miss-identified with it.

A total of 10^{-6} events were simulated for every decay studied. All hadrons were configured to have LHCb generic smear to represent the effect of imperfect track reconstruction.

The final state particles of every missidentified hadronic decay were swapped as follows: Two oppositely charged hadrons were missID with the electron-positron pair of the signal, while the remaining hadrons were identified as K^+ and π^- respectively.

Several mass vetoes were applied to the simulated data to see the effect of this miss-identification on the regions of interest.

3.2 Signal

This thesis focused on the study of the signal $B^0 \to K^+\pi^-e^+e^-$.

The combined mass of the final state particles $K^+\pi^-e^+e^-$ is constrained to the mass of initial state B^0, thus we narrowed the B^0 mass to the region $4.5 < m(B^0) < 6.0$ GeV/c^2. As discussed in section 2.3, the invariant $K\pi$ mass and the dilepton squared mass regions were constrained to $992 < m(K\pi) < 2600$ MeV/c^2 and $1.1 < q^2 < 7.0$ GeV$^2/c^4$ respectively.

To estimate the amount of signal events in the region of interest, first an estimation of the branching fraction of the decay was computed. A good estimation of the branching fraction Γ of the signal $B^0 \to K^+\pi^-e^+e^-$ was obtained from previous LHCb measurements of its sister signal $B^0 \to K^+\pi^-\mu^+\mu^-$.

The behaviour of the $B^0 \to K^+\pi^-\mu^+\mu^-$ has been previously accurately measured for the of the analysis of the $R_{K^{*0}}$ in 2017.[2].

As previously discussed the $R_{K^{*0}}$ ratio was measured for $m(K\pi)$ in the region $792 < m(K\pi) < 992$ MeV/c^2. From figure 3.1 we are able to compute the ratio of $B^0 \to K^+\pi^-\mu^+\mu^-$ decays between this region and the region $992 < m(K\pi) < 2600$ MeV/c^2. This estimation was made by measuring the areas obtained from

q^2 (GeV^2/c^4)	$N_{\mathbf{sig}}$	$\mathrm{d}\mathcal{B}/\mathrm{dII}^{\in}$ ($10^{-7}\,\mathrm{GeV}^{-2}c^4$)
0.10 − 2.00	140 ± 13	$0.60 \pm 0.06 \pm 0.05 \pm 0.04\,^{+0.00}_{-0.05}$
2.00 − 4.30	73 ± 11	$0.30 \pm 0.03 \pm 0.03 \pm 0.02\,^{+0.00}_{-0.02}$
4.30 − 8.68	271 ± 19	$0.49 \pm 0.04 \pm 0.04 \pm 0.03\,^{+0.00}_{-0.04}$
10.09 − 12.86	168 ± 15	$0.43 \pm 0.04 \pm 0.04 \pm 0.03\,^{+0.00}_{-0.03}$
14.18 − 16.00	115 ± 12	$0.56 \pm 0.06 \pm 0.04 \pm 0.04\,^{+0.00}_{-0.05}$
16.00 − 19.00	116 ± 13	$0.41 \pm 0.04 \pm 0.04 \pm 0.03\,^{+0.00}_{-0.03}$
1.00 − 6.00	197 ± 17	$0.34 \pm 0.03 \pm 0.04 \pm 0.02\,^{+0.00}_{-0.03}$

Table 3.1: Signal yield ($Nsig$) and differential branching fraction ($d\mathcal{B}/dq^2$) of the $B^0 \to K^{*0}\mu^+\mu$ decay for different q^2 bins in the $792 < m(K^+\pi) < 992$ MeV/c^2 mass window.[5]

figure 3.1 that is part of the LHCb public results[4], resulting in the following ratio:

$$R_{K\pi\ decays} = \frac{792 < m(K^+\pi^-) < 992 \ \ \mathrm{MeV}/c^2}{992 < m(K^+\pi^-) < 2600 \ \ \mathrm{MeV}/c^2} = 1.22 \tag{3.1}$$

The differential branching fraction $d\mathcal{B}/dq^2$ of $B^0 \to K^{*0}\mu^+\mu^-$ for a dilepton mass squared between 1.1 and 6.0 GeV^2/c^4 was obtained from information extracted from table 3.1 that is also part of the LHCb public results.[5]

$$\left.\frac{d\mathcal{B}}{dq^2}\right|_{1.0<q^2<6.0} \approx 0.34 \cdot 10^{-7}\ \mathrm{GeV}^{-2}/c^4 \tag{3.2}$$

The estimation of the branching fraction for the electron was obtained by multiplying the differential branching fraction of the muon channel and the ratio of decays of the corresponding $m(K\pi)$. To expand the q^2 window from 6.0 to 7.0 GeV^2/c^4, the previous result was multiplied by the difference between the ratio of the two regions:

$$\begin{aligned}\Gamma_{signal} &= \left(\frac{d\mathcal{B}}{dq^2}\Big|_{1.0<q^2<6.0}\right) \cdot \underbrace{\left(\frac{7.0-1.1}{6.0-1.1}\right)}_{\text{to shift } q^2} \cdot (R_{K\pi\ decays}) \\ &= 1.7687 \cdot 10^{-7}\end{aligned} \tag{3.3}$$

To calculate the expected number of signal events, i.e. the number of signal events in the regions of interest expected from the RapidSim simulated data, the efficiency of the signal after applying the mass vetoes was computed resulting on a remaining 40.05% of events surviving the mass vetoes. However given that

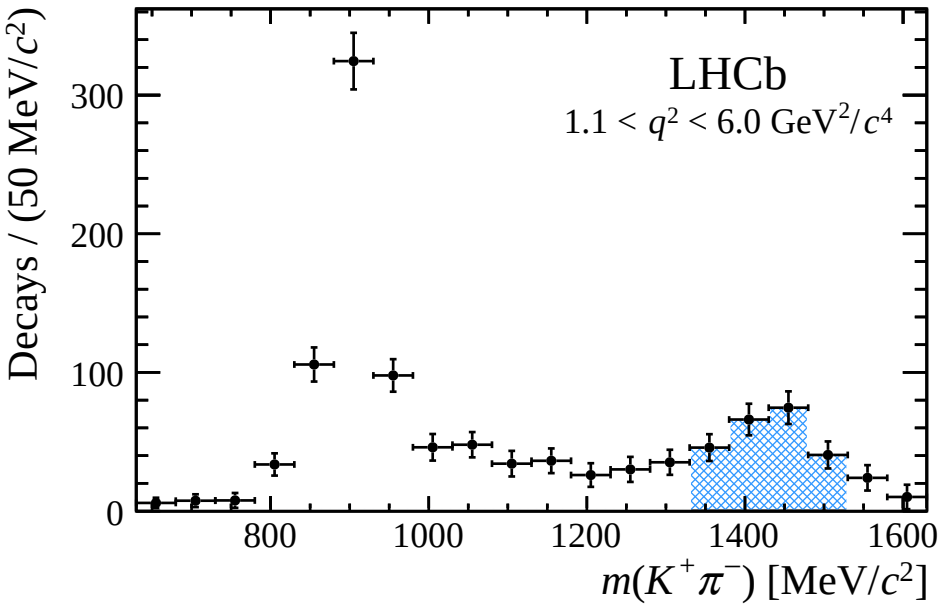

Figure 3.1: Background-subtracted $m(K^+\pi)$ distribution for $B^0 \to K^+\pi^-\mu^+\mu^-$ decays in the range $1.1 < q^2 < 6.0$ GeV$^2/c^4$. The region $1330 < m(K^+\pi) < 1530$ MeV$/c^2$ is indicated by the blue, hatched area.[4]

we generated the signal specifically within the $m(K\pi)$ and q^2 constrains, the efficiency of the signal considered future computations was of 100%. In table 3.2 we can see a summary of the results obtained.

Decay	Γ $[10^{-7}]$	**Eff.** [%]	**Number of Events** $[10^{-5}]$
$B^0 \to K^+ \pi^- e^+ e^-$	1.7687	100	1.7687

Table 3.2: The resulting branching fraction Γ of the signal was estimated using previous LHCb public measurements. The expected number of events in the signal region was computed to be on the order of 10^{-5}.

3.3 Electron-Hadron Missidentification

The LHCb experiment is able to detect trillions of decays. A challenge of any type of analysis of the data collected by this experiment is to be able to reconstruct and identify the decays matching the desired signal events.

For a specific B meson decay, the detector records the resulting final state particles and uses them to reconstruct the initial state of the mother particle. The decay is reconstructed based on a series of kinematic and physical constraints built using theoretical SM predictions.

In the case of $B^0 \to K^+\pi^-e^+e^-$, the B^0 candidate is reconstructed from a pair of well-reconstructed oppositely charged particles identified as electrons, combined with two well-reconstructed oppositely charged particles, one identified as a kaon K and the other as a pion π.

The B^0 mass resolution and the contributions of signal and backgrounds depends in part in the correct particle identification (PID). The separation between π^0 and γ, or between a π^+ and a K^+, or between a π^- and e^- is vital to the reconstruction of the B^0 candidate that is been studied.

Even after an exhaustive series of pre-selecction requirement applied to the data.[16] A series of backgrounds that cannot be reduced nor rule out remain as a source of contamination due to the miss identification between hadron and leptons, this effect is more pronounce in the case of electrons as seen in section 2.6.

The objective of this thesis is to provide a preliminary analysis of the contamination of these type of irreducible background on the case of $B^0 \to K^+\pi^-e^+e^-$.

3.4 Irreducible Backgrounds

There are several B meson decays resulting in hadronic final state particles that can be missidentified as a signal event. Such decays include cases where the final states can be missID with either the K^+, the π^- or with electron-positron pair. The probability of hadron-electron missID is 1%.

A list of all the possible decays that could be missID with the signal was extracted from the particle data group (PDG) archive.[18] The B mesons considered included B^0, B_s and B^+.

All these B mesons decays, with every intermediate decay channels that resulted in at least four oppositely charged particles are listed in table 3.3 together with the corresponding branching fractions Γ of every intermediate transition.

Decays	**1**st Γ $\left[10^{-6}\right]$	**2**nd Γ	**3**rd Γ
$B^0 \to \{ K^{*0} \to K^+ \pi^- \} \{ \eta' \to \pi^+ \pi^- \eta \}$	2.80	1.00	0.43
$B^0 \to \{ K^{*0} \to K^+ \pi^- \} \{ \eta' \to \pi^+ \pi^- \gamma \}$	2.80	1.00	0.29
$B^0 \to \{ K_0^*(1430)^0 \to K^+ \pi^- \} \{ \eta' \to \pi^+ \pi^- \eta \}$	6.30	0.93	0.43
$B^0 \to \{ K_0^*(1430)^0 \to K^+ \pi^- \} \{ \eta' \to \pi^+ \pi^- \gamma \}$	6.30	0.93	0.29
$B^0 \to \{ K_2^*(1430)^0 \to K^+ \pi^- \} \{ \eta' \to \pi^+ \pi^- \eta \}$	13.70	0.50	0.43
$B^0 \to \{ K_2^*(1430)^0 \to K^+ \pi^- \} \{ \eta' \to \pi^+ \pi^- \gamma \}$	13.70	0.50	0.29
$B^0 \to \{ K^{*0} \to K^+ \pi^- \} \{ \eta \to \pi^+ \pi^- \pi^0 \}$	15.90	1.00	0.23
$B^0 \to \{ K_0^*(1430)^0 \to K^+ \pi^- \} \{ \eta \to \pi^+ \pi^- \pi^0 \}$	11.00	0.93	0.23
$B^0 \to \{ K_2^*(1430)^0 \to K^+ \pi^- \} \{ \eta \to \pi^+ \pi^- \pi^0 \}$	9.60	0.50	0.23
$B^0 \to \{ K^{*0} \to K^+ \pi^- \} \{ \omega \to \pi^+ \pi^- \pi^0 \}$	2.00	1.00	0.89
$B^0 \to \{ K^{*0} \to K^+ \pi^- \} \{ \omega \to \pi^+ \pi^- \pi^0 \}$	18.40	1.00	0.89
$B^0 \to \{ K_0^*(1430)^0 \to K^+ \pi^- \} \{ \omega \to \pi^+ \pi^- \pi^0 \}$	16.00	0.93	0.89
$B^0 \to \{ K_2^*(1430)^0 \to K^+ \pi^- \} \{ \omega \to \pi^+ \pi^- \pi^0 \}$	10.10	0.50	0.89
$B^0 \to K^+ \pi^- \{ \omega \to \pi^+ \pi^- \pi^0 \}$	5.10	1.00	0.89
$B^0 \to K^+ \pi^- \{ \rho^0 \to \pi^+ \pi^- \}$	2.80	1.00	1.00
$B^0 \to K^+ \pi^- \{ f_0(980) \to \pi^+ \pi^- \}$	1.40	1.00	1.00
$B^0 \to \{ K^{*0} \to K^+ \pi^- \} \pi^+ \pi^-$	55.00	1.00	1.00
$B^0 \to \{ K^{*0} \to K^+ \pi^- \} \{ \rho^0 \to \pi^+ \pi^- \}$	3.90	1.00	1.00
$B^0 \to \{ K^{*0} \to K^+ \pi^- \} \{ f_0(980) \to \pi^+ \pi^- \}$	3.90	1.00	1.00
$B^0 \to \{ K_0^*(1430)^0 \to K^+ \pi^- \} \{ \rho^0 \to \pi^+ \pi^- \}$	27.00	0.93	1.00
$B^0 \to \{ K_0^*(1430)^0 \to K^+ \pi^- \} \{ f_0(980) \to \pi^+ \pi^- \}$	2.70	0.93	1.00
$B^0 \to \{ K_2^*(1430)^0 \to K^+ \pi^- \} \{ f_0(980) \to \pi^+ \pi^- \}$	8.60	0.50	1.00
$B^0 \to \{ K^{*0} \to K^+ \pi^- \} K^+ K^-$	27.50	1.00	1.00
$B^0 \to \{ K^{*0} \to K^+ \pi^- \} \{ \phi \to K^+ K^- \}$	10.00	1.00	0.49
$B^0 \to \{ K^{*0} \to K^+ \pi^- \} \{ \phi \to \pi^+ \pi^- \}$	10.00	1.00	< 0.01
$B^0 \to \{ K^{*0} \to K^+ \pi^- \} K^- \pi^+$	4.50	1.00	1.00
$B^0 \to \{ K^{*0} \to K^+ \pi^- \} \{ \overline{K}^{*0} \to K^- \pi^+ \}$	0.80	1.00	1.00
$B^0 \to \{ K_0^*(1430)^0 \to K^+ \pi^- \} \{ \phi \to K^+ K^- \}$	3.90	0.93	0.49
$B^0 \to \{ K_0^*(1430)^0 \to K^+ \pi^- \} \{ \phi \to \pi^+ \pi^- \}$	3.90	0.93	< 0.01
$B^0 \to \{ K_2^*(1430)^0 \to K^+ \pi^- \} \{ \phi \to K^+ K^- \}$	6.80	0.93	0.49
$B^0 \to \{ K_2^*(1430)^0 \to K^+ \pi^- \} \{ \phi \to \pi^+ \pi^- \}$	6.80	0.93	< 0.01
$B^0 \to K^0 \{ \phi \to K^+ K^- \} \{ \phi \to K^+ K^- \}$	3.10	0.49	0.49
$B^0 \to K^0 \{ \phi \to \pi^+ \pi^- \} \{ \phi \to \pi^+ \pi^- \}$	3.10	< 0.01	< 0.01
$B^0 \to K^0 \{ \phi \to K^+ K^- \} \{ \phi \to \pi^+ \pi^- \}$	3.10	0.49	< 0.01
$Bs^0 \to \{ \phi \to K^+ K^- \} \{ f_0(980) \to \pi^+ \pi^- \}$	1.12	0.49	1.00
$Bs^0 \to \{ \phi \to \pi^+ \pi^- \} \{ f_0(980) \to \pi^+ \pi^- \}$	1.12	< 0.01	1.00
$Bs^0 \to \{ \phi \to K^+ K^- \} \{ f_2(1270) \to \pi^+ \pi^- \}$	0.61	0.49	0.84
$Bs^0 \to \{ \phi \to \pi^+ \pi^- \} \{ f_2(1270) \to \pi^+ \pi^- \}$	0.61	< 0.01	0.84
$Bs^0 \to \{ \phi \to K^+ K^- \} \{ \rho^0 \to \pi^+ \pi^- \}$	0.27	0.49	1.00
$Bs^0 \to \{ \phi \to \pi^+ \pi^- \} \{ \rho^0 \to \pi^+ \pi^- \}$	0.27	< 0.01	1.00
$Bs^0 \to \{ \phi \to K^+ K^- \} \pi^+ \pi^-$	3.50	0.49	1.00
$Bs^0 \to \{ \phi \to \pi^+ \pi^- \} \pi^+ \pi^-$	3.50	< 0.01	1.00
$Bs^0 \to \{ \phi \to K^+ K^- \} \{ \phi \to \pi^+ \pi^- \}$	18.50	0.49	< 0.01
$Bs^0 \to \{ \phi \to \pi^+ \pi^- \} \{ \phi \to K^+ K^- \}$	18.50	< 0.01	0.49
$Bs^0 \to \{ K^{*0} \to K^+ \pi^- \} \{ \overline{K}^{*0} \to K^- \pi^+ \}$	11.10	1.00	1.00

Continued on next page

Decays	$\mathbf{1}^{st}\ \Gamma\ [10^{-6}]$	$\mathbf{2}^{nd}\ \Gamma$	$\mathbf{3}^{rd}\ \Gamma$
$Bs^0 \to \{ K^{*0} \to K^+ \pi^- \} \{ \phi \to K^+ K^- \}$	1.14	1.00	0.49
$Bs^0 \to \{ K^{*0} \to K^+ \pi^- \} \{ \phi \to \pi^+ \pi^- \}$	1.14	1.00	< 0.01
$B^+ \to K^+ \{ \phi \to \pi^+ \pi^- \} \{ \phi \to K^+ K^- \}$	4.20	< 0.01	0.49
$B^+ \to K^+ \{ \phi \to \pi^+ \pi^- \} \{ \phi \to K^+ K^- \}$	4.20	< 0.01	0.49
$B^+ \to K^+ \{ \phi \to \pi^+ \pi^- \} \{ \phi \to \pi^+ \pi^- \}$	4.20	< 0.01	< 0.01

Table 3.3: List of all possible irreducible B meson decays whose final state particles can be missID with the signal. The $\mathbf{1}^{st}\ \Gamma$ corresponds to the branching fraction of the mother particle to the first intermediate state (from left to right). The $\mathbf{2}^{nd}\ \Gamma$ and $\mathbf{3}^{rd}\ \Gamma$ corresponds to the branching fractions of second intermediate state. A branching fraction of 1 was assigned to the states that did not have a secondary intermediate state.

The total branching fraction, this is the branching fraction of the decays through the specific decay channels listed in table 3.3 was computed by multiplying the branching fractions of each intermediate channel. Of these, only a subset of 10 decays with the largest total branching fractions were used in this analysis, see table 3.4.

As an example, for the decay:

$$B^0 \to \{K^{*0} \to K^+\pi^-\}\{\phi \to K^+K^-\}$$

The $1^{st}\Gamma$ corresponds to the branching fraction of the process $B^0 \to K^{*0}\phi$, the $2^{nd}\Gamma$ corresponds to that of the process $K^{*0} \to K^+\pi^-$ and the $3^{rd}\Gamma$ corresponds to $\phi \to K^+K^-$.

For this decay, there are two possible miss identification scenarios:

- $B^0 \to \{K^{*0} \to K^+\pi^-\}\{\phi \to K^+_{\to e^+}K^-_{\to e^-}\}$
- $B^0 \to \{K^{*0} \to K^+_{\to e^+}\pi^-\}\{\phi \to K^+K^-_{\to e^-}\}$

Similarly, the ordering on the list of decays in table 3.4 corresponds to the electron miss identification of hadrons in this order, when two possibilities for missID are available.

3.5 Mass Vetoes

As to be able to study the contribution of the irreducible backgrounds to the signal $K^+\pi^-e^+e^-$ in the region of interest, several mass vetoes were applied. The mass of the mother particle, the B meson, was constrained to the mass of B^0, i.e. to the region $4.5 < m(B^0) < 6.0$ GeV/c^2.

The mass of $K\pi$ was reduced to the unexplored region $992 < m(K\pi) < 2600$ MeV/c^2, and the dilepton squared mass of the electron was constrained to $1.1 < q^2 < 7.0$ GeV/c^2. The number of events remaining after applying this mass window together with the probability of hadron-electron missidentification[3] were used to compute the efficiency of these vetoes on each of the backgrounds.

To estimate the expected number of final events, **N.E.** of each background, the efficiency, **Eff.** computed from the simulation, and the total branching fraction Γ of each specific channel was multiplied. The results are presented in table 3.4.

Decays	Γ $[10^{-6}]$	**Eff.** [%]	**N.E.** $[10^{-12}]$
$B^0 \to \{ K^{*0} \to K^+ \pi^- \} \pi^+ \pi^-$	55.00	4.10	225.55
$B^0 \to \{ K^{*0} \to K^+ \pi^- \} \pi^+ \pi^-$	55.00	3.67	201.85
$B^0 \to \{ K^{*0} \to K^+ \pi^- \} K^+ K^-$	27.50	4.61	126.79
$B^0 \to \{ K^{*0} \to K^+ \pi^- \} K^+ K^-$	27.50	1.47	40.43
$B^0 \to \{ K_0^*(1430)^0 \to K^+ \pi^- \} \{ \rho^0 \to \pi^+ \pi^- \}$	25.11	12.04	302.21
$B^0 \to \{ K^{*0} \to K^+ \pi^- \} \{ \omega \to \pi^+ \pi^- \pi^0 \}$	16.41	~ 0	~ 0
$B^0 \to \{ K^{*0} \to K^+ \pi^- \} \{ \omega \to \pi^+ \pi^- \pi^0 \}$	16.41	~ 0	~ 0
$B^0 \to \{ K_0^*(1430)^0 \to K^+ \pi^- \} \{ \omega \to \pi^+ \pi^- \pi^0 \}$	13.27	~ 0	~ 0
$B^0 \to \{ K_0^*(1430)^0 \to K^+ \pi^- \} \{ \omega \to \pi^+ \pi^- \pi^0 \}$	13.27	~ 0	~ 0
$Bs^0 \to \{ K^{*0} \to K^+ \pi^- \} \{ \overline{K}^{*0} \to K^- \pi^+ \}$	11.10	0.21	2.33
$B^0 \to \{ K^{*0} \to K^+ \pi^- \} \{ \phi \to K^+ K^- \}$	4.89	0.04	0.20
$B^0 \to \{ K^{*0} \to K^+ \pi^- \} \{ \phi \to K^+ K^- \}$	4.89	0.01	0.05
$B^0 \to K^+ \pi^- \{ \omega \to \pi^+ \pi^- \pi^0 \}$	4.55	~ 0	~ 0
$B^0 \to K^+ \pi^- \{ \omega \to \pi^+ \pi^- \pi^0 \}$	4.55	~ 0	~ 0
$B^0 \to \{ K^{*0} \to K^+ \pi^- \} K^- \pi^+$	4.50	2.50	11.25
$B^0 \to \{ K_2^*(1430)^0 \to K^+ \pi^- \} \{ \omega \to \pi^+ \pi^- \pi^0 \}$	4.50	~ 0	~ 0
$B^0 \to \{ K_2^*(1430)^0 \to K^+ \pi^- \} \{ \omega \to \pi^+ \pi^- \pi^0 \}$	4.50	~ 0	~ 0

Table 3.4: Summary of the top ten irreducible backgrounds according to largest branching fractions Γ. For decays where two possibilities for hadron-electtron missID are available, the missidentifications was made following the order outlined in section 3.4. **Eff.** is efficiency of the mass vetoes and **N.E.** is the expected number of events for each missidentification.

[3] The probability of hadron-electron missidentification is 1%.

3.6 Fitting Analysis

The signal yield was determined by using an unbinned extended maximum likelihood fit of the four-body invariant mass, $m(K^+\pi^-e+e)$, of the selected candidates after applying the corresponding $m(K\pi)$ and q^2 mass vetoes.

The signal shape is broad due to the electron bremsstrahlung emitted, thus the probability density function (PDF) of the signal was described using the sum of two Crystal Ball (CB) functions, otherwise know as a double Crystal Ball (DCB) distribution.[2] A DCB is defined as:

$$f\left(x,\mu,\sigma,\alpha_L,n_L,\alpha_R,n_R\right) = \begin{cases} A_L\left(B_L - \frac{x-\mu}{\sigma}\right)^{-n_L}, & \frac{x-\mu}{\sigma} < \alpha_L \\ exp\left(-\frac{(x-\mu)^2}{2\sigma^2}\right), & -\alpha_L \leq \frac{x-\mu}{\sigma} \leq \alpha_R \\ A_R\left(B_R - \frac{x-\mu}{\sigma}\right)^{-n_R}, & \frac{x-\mu}{\sigma} > \alpha_R \end{cases}$$

where:

$$A_i = \left(\frac{n_i}{|\alpha_i|}\right)^{n_i} exp(-\frac{|\alpha^2|}{2}) \quad \text{for } i = L, R$$
$$B_i = \frac{n_i}{|\alpha_i|} - |\alpha_i|$$

This distribution consists of a Gaussian core, modelling the resolution of the detector, with power-law tails on each side. The left hand tail of the DCB function takes final state radiation (FSR) and interaction with matter into account while the right hand tail describes non-gaussian detector effects. A relinquishment of the right hand tail (i.e. the use of a single CB) could result in a bias of the mean as well as of the sigma of the Gaussian.

The parameters μ and σ define the center and width of the Gaussian. The parameters α_L and α_R determine the transition point between the Gaussian and the power-laws with the exponents n_L and n_R, on the right and left side respectively.

The fits are performed using the maximum likelihood principle: Given a PDF $F(x;a)$ that models the behaviour of the dataset x, and is is parameterised by a; the likelihood L of the fit is defined as the probability that the model assigns to the data sample $(x_1, ..., x_N)$:

$$L(x_1, ..., x_N; a) = \prod_i F(x_i; a) \tag{3.4}$$

The optimal parameters $\hat{a}$ are determined in order to maximise this likelihood, in other words, as to maximise the probability for the data sample to be described by the given model.

To obtain an unbinned extended maximum likelihood fit of the four-body invariant mass of $m(K^+\pi^-e+e)$, of the previously selected candidates after the selection of the corresponding $m(K\pi)$ and q^2 regions, reasonable initial parameters need to be provided to the fit.

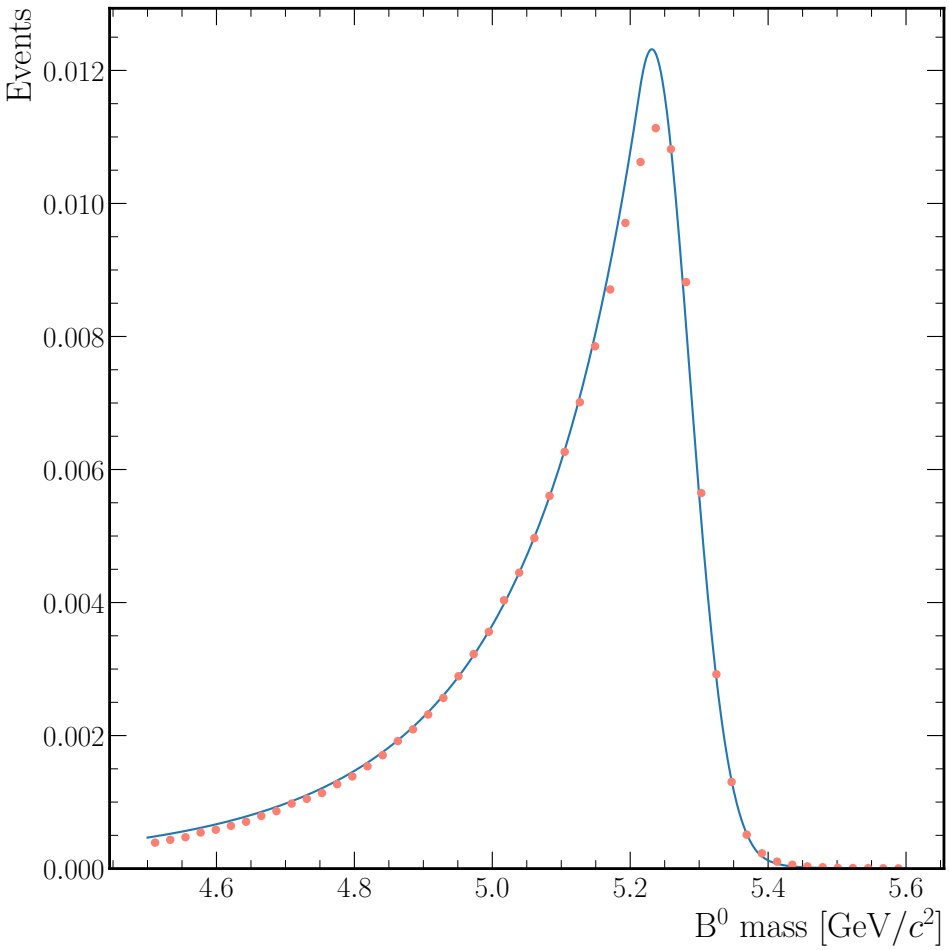

Figure 3.2: DCB fit of a pure simulated sample of the signal $B^0 \to K^+\pi^-e^+e^-$. A total of 10^6 events were simulated using RapidSim. The smearing effect of the resulting electrons and hadrons were included in the simulation.

In order to optimise the choice of the initial parameters of the fit, a DCB distribution was fitted to pure signal sample generated in RapidSim. The smearing effects of hadrons and electrons were included. The result of the fit is shown in figure 3.2, and the parameters found are shown in table 3.6. The inclusion of the smearing effects of the detector in the simulation can be seen on the quality of the fit around the peak.

After applying the mass vetoes as discussed in section 3.5, the remaining signal and background were fitted using a DCB with the initial parameters obtained from the raw signal fit. The resulting fit can be seen in figure 3.3. The signal peak can be observed, albeit with a relatively large relative uncertainty after applying the mass vetoes. The values of the parameters obtained from this fit can be found in table 3.6.

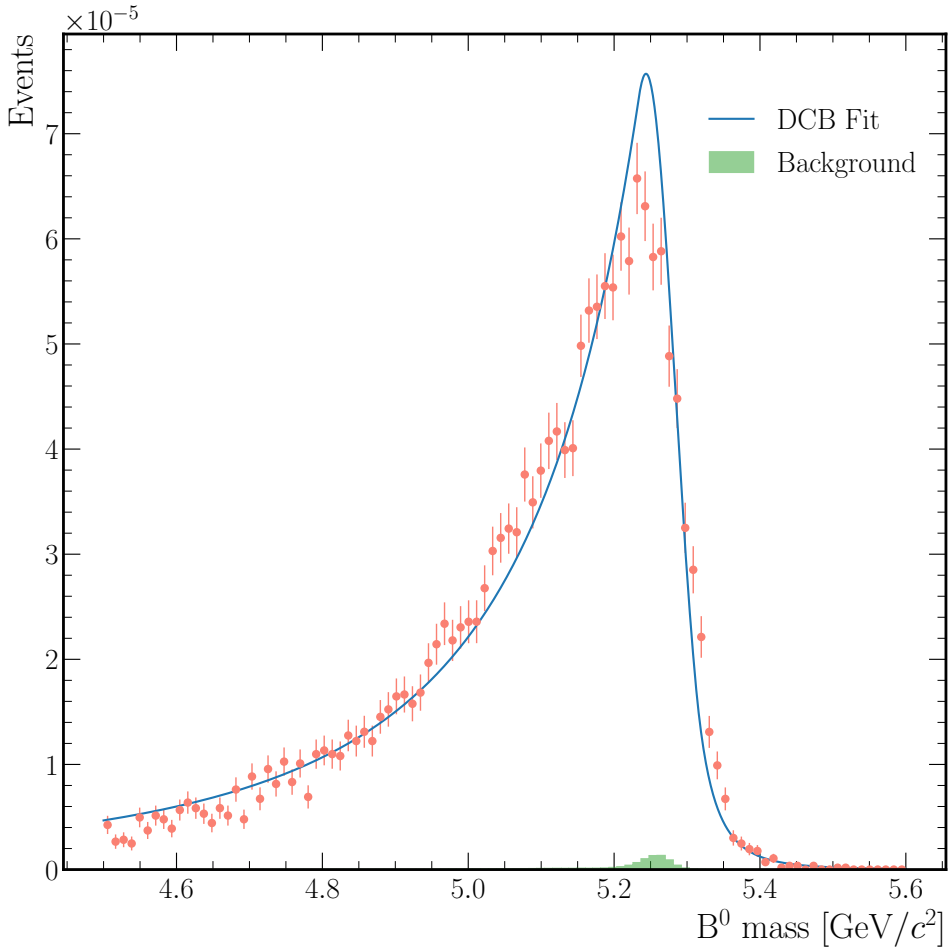

Figure 3.3: DCB fit to the candidate $B0 \to K^+\pi^-e^+e$. The contributions of the missID hadronic backgrounds are shown shaded in green.

3.7 Discussion and Results

Branching Fraction Analysis: The estimated branching fraction of the signal $B^0 \to K^+\pi^-e^+e^-$ is on the order of 10^{-7}, while the the branching fractions of the hadronic missID backgrounds are on the order of 10^{-6}. See tables 3.2 and 3.4. Given the similar order of magnitude of the branching fractions, the ratio of signal to background of expected events is determined mostly by the efficiency of the mass vetoes.

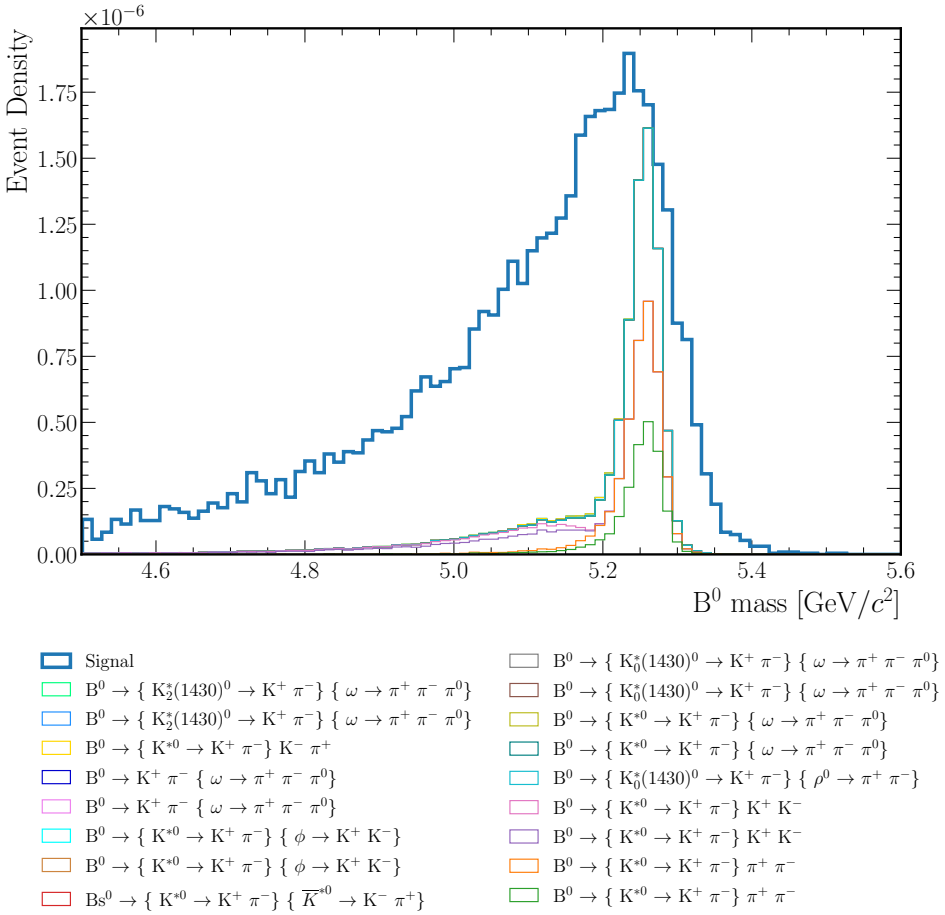

Figure 3.4: Stacked histogram of the expected event density of missID hadronic backgrounds. The signal, $B^0 \to K^+\pi^-e^+e^-$ is in blue. The number of signal events has been scaled down to 2.5% to offer a visual comparison between the hadronic missID backgrounds on the B^0 mass region.

Efficiency of the Mass Selection: The mass vetoes significantly reduced the number events corresponding to the missID hadronic backgrounds. In figure 3.4 the shape and the location of the remaining events is shown. To present a visual comparison with the signal, the size of the signal was reduced by 97.5%.

The signal yield, defined here as the signal to background ratio[4] of the number of events before and after the mass vetoes were applied shows the increased efficiency of this selection on the elimination of the number of events produced by hadronic missID. See table 3.5.

Mass Selection	**Signal Yield**
Before	0.000604
After	0.994878

Table 3.5: Effect of the mass selection on the signal yield.

Fitting Analysis: Figure 3.2 shows the DCB fit of the pure $B^0 \to K^+\pi^-e^+e^-$ signal simulated by RapidSim. The reconstructed B^0 mass was 5.252 GeV/c^2 with a standard deviation of 38.94 MeV/c^2. The fit performed after the mass selection is shown in figure 3.3. The four-body invariant mass B^0 obtained from the fit was 5.244 GeV/c^2 with a standard deviation of 39.94 MeV/c^2.

The remaining parameters obtained by the DCB fit are shown in table 3.6. The distribution seem to fit accurately the tails of the DCB model, corresponding to the power law description of the FSR and matter interaction, and the non gaussian detector effects on the left and right side respectively.

Fit Parameters	**Pure Signal**	**Candidate Signal**	**Units**
α_L	0.22910	0.25590	—
n_L	5.89100	2.78200	—
α_R	1.83300	1.70200	—
n_R	3.04900	4.08900	—
μ	5.25200	5.24400	$[\text{GeV}/c^2]$
σ	0.03894	0.03994	$[\text{GeV}/c^2]$

Table 3.6: On the left Parameters obtained from the DCB fit to the full signal, on the right parameters obtained after the mass selection.

[4]The signal to background ratio is defined as $\left(\frac{s}{s+b}\right)$, where s is the number of signal events and b, the number of background events.

Leakage of the missID Hadronic Backgrounds: The main leakage region is located on the lower $m(K\pi)$ region with a secondary peak around 1.4 GeV/c^2, see figure 3.5. Similarly, figure 3.6 shows the largest leakage occurring on the lower q^2 region.

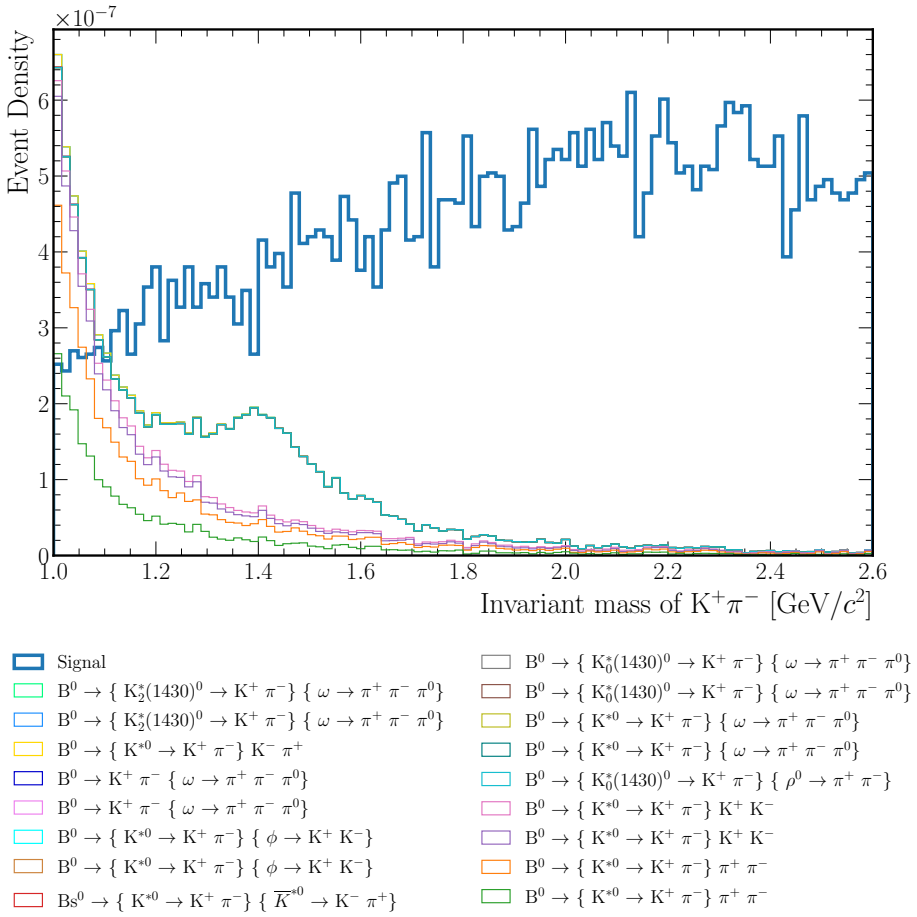

Figure 3.5: Histogram of the $m(K^+\pi)$ distribution of the signal and missID hadronic backgrounds in the range $1.1 < q^2 < 7.0$ GeV$^2/c^4$. The signal is in blue. The number of signal events has been scaled to 2.5%, as to offer a visual comparison of the contaminated region.

The largest contribution of this leakage comes from the missidentification of the first π^- with an e^- and the second π^+ with a positron e^+ in the hadronic process $B^0 \to \{K^{*0} \to K^+\pi^-_{\to e^-}\}\{\omega \to \pi^+_{\to e^+}\pi^-\pi^0\}$. The contributions of the remaining missidentified hadronic process are of a similar order.

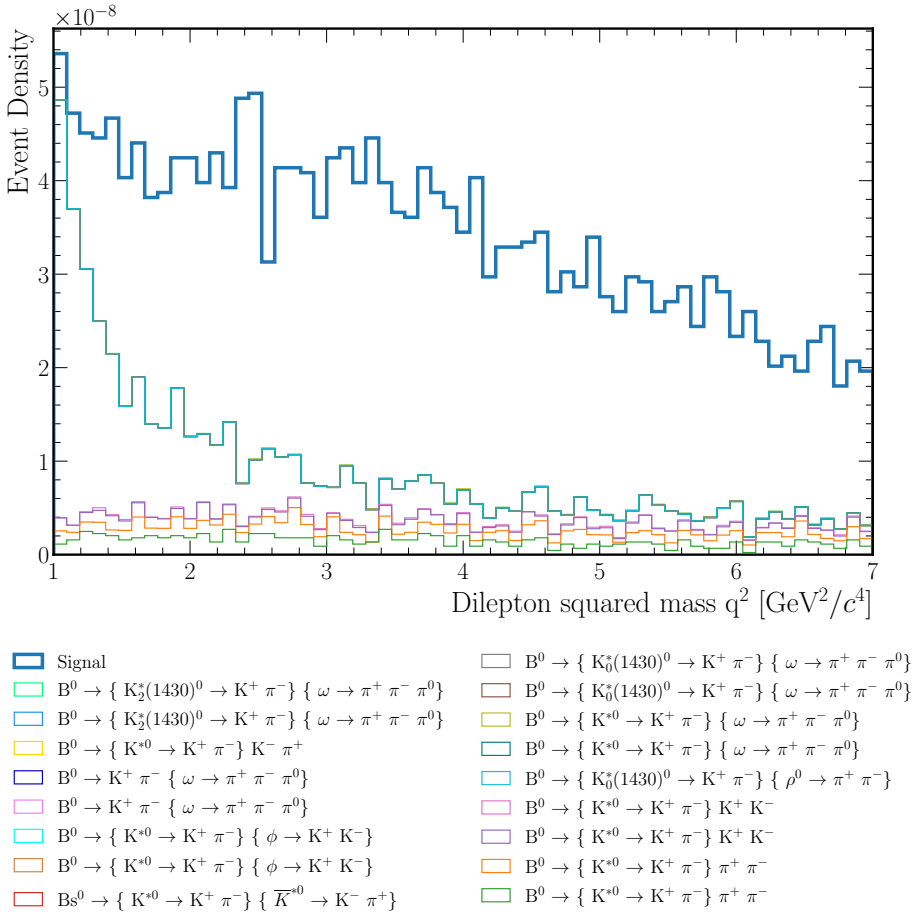

Figure 3.6: Background-subtracted q^2 distribution for the signal and the irreducible decays. The signal has been scaled by 2.5% to offer a visual comparison with the irreducible decays.

Although the contributions of these process are minimal in the signal region, accounting for their effects could help to establish a tighter electron identification criteria, or to a better modelling of the residual misidentified hadronic backgrounds.

Conclusion

Previous results of the measurement of the $R_{K^{0}*}$ ratio indicate evidence for the breaking of lepton universality in beauty-quark decays, and while as mentioned on this thesis, the statistical sensitivity of these measurements is small, a coherent pattern on the measurement of these deviations calls for further analysis of these decays, be it to corroborate or exclude these findings.

Three days before the handling of this thesis, on December 20, 2022, the LHCb Collaboration presented fresh new results on the measurement of the $R_{K^{0}*}$ ratio. The new results differ with the deviations observed in the previous analysis published in 2017. Although the same dataset was used the difference on the results is accounted by the use of tighter electron identification criteria and a better modelling of the residual misidentified hadronic backgrounds.

These new results highlight the need of further improvements on the modelling and identification of electron signals in beauty-quark decays at the LHCb. Furthermore, these results cement the need to extend this analysis to the unexplored regions of $m(K\pi)$.

While the results presented on this thesis can be used as a a preliminary analysis in the modelling of electron-hadron missidentification, further analysis should be performed using complete phase space simulations as to gauge the limitations and advantages of RapidSim.

Whilst RapidSim offers a fast and robust way to study the properties of B meson decays involving electrons, accounting even for the electron smearing effects of the detector. Given that small statistical fluctuations can have significant effects on the modelling of missidentified hadronic backgrounds, even small contributions, like the ones studied on this thesis could result in higher precision measurements of the electron channel. Thus further understanding on their contaminating effects is needed.

Bibliography

[1] "Standard model of physics representation," http://davidgalbraith.org/portfolio/ux-standard-model-of-the-standard-model/, accessed: 2022-12-16.

[2] A. Camboni, S. Coquereau, G. Fernandez, L. Garrido Beltrán, D. Gascon, R. Graciani Diaz, C. Marin Benito, E. Picatoste Olloqui, V. Rives Molina, D. Sanchez Gonzalo *et al.*, "Test of lepton universality with b 0→ k* 0 + -decays," *Journal of High Energy Physics, 2017, vol. 2017, num. 55, p. 1-31*, 2017.

[3] A. A. Alves Jr, L. Andrade Filho, A. Barbosa, I. Bediaga, G. Cernicchiaro, G. Guerrer, H. Lima Jr, A. Machado, J. Magnin, F. Marujo *et al.*, "The lhcb detector at the lhc," *Journal of instrumentation*, vol. 3, no. 08, p. S08005, 2008.

[4] A. Camboni, L. Garrido Beltrán, D. Gascón Fora, R. Graciani Díaz, C. Marin Benito, E. Picatoste Olloqui, V. J. Rives Molina, A. Badalov, L. Collaboration *et al.*, "Differential branching fraction and angular moments analysis of the decay b 0→ k+ π- μ+ μ- in the k 0, 2(1430) 0 region," *Journal of High Energy Physics, 2016, vol. 2016, num. 65*, 2016.

[5] R. Aaij, C. A. Beteta, B. Adeva, M. Adinolfi, C. Adrover, A. Affolder, Z. Ajaltouni, J. Albrecht, F. Alessio, M. Alexander *et al.*, "Differential branching fraction and angular analysis of the decay b 0→ k* 0 μ+ μ-," *Physical review letters*, vol. 108, no. 18, p. 181806, 2012.

[6] M. E. Peskin, *An introduction to quantum field theory*. CRC press, 2018.

[7] M. Kirk, "Cabibbo anomaly versus electroweak precision tests: An exploration of extensions of the standard model," *Physical Review D*, vol. 103, no. 3, p. 035004, 2021.

[8] W. Altmannshofer, J. Davighi, and M. Nardecchia, "Gauging the accidental symmetries of the standard model, and implications for the flavor anomalies," *Physical Review D*, vol. 101, no. 1, p. 015004, 2020.

[9] N. Cabibbo, "Unitary symmetry and leptonic decays," *Physical Review Letters*, vol. 10, no. 12, p. 531, 1963.

[10] T. E. Browder and K. Honscheid, "B mesons," *Progress in Particle and Nuclear Physics*, vol. 35, pp. 81–219, 1995.

[11] R. Alonso, B. Grinstein, and J. M. Camalich, "Lepton universality violation with lepton flavor conservation in b-meson decays," *Journal of High Energy Physics*, vol. 2015, no. 10, pp. 1–30, 2015.

[12] R. Bernet, K. Müller, O. Steinkamp, U. Straumann, A. Vollhardt, L. Collaboration *et al.*, "Implications of lhcb measurements and future prospects," *European Physical Journal C-Particles and Fields*, vol. 73, p. 2373, 2013.

[13] "Test of lepton universality in beauty-quark decays," *Nature Physics*, vol. 18, no. 3, pp. 277–282, 2022.

[14] L. Collaboration, "Test of lepton universality with b 0 k* 0+ decays," *JHEP*, vol. 8, p. 055, 2017.

[15] C. Bobeth, G. Hiller, and G. Piranishvili, "Angular distributions of b→ kll decays," *Journal of High Energy Physics*, vol. 2007, no. 12, p. 040, 2007.

[16] R. Aaij, C. A. Beteta, T. Ackernley, B. Adeva, M. Adinolfi, H. Afsharnia, C. A. Aidala, S. Aiola, Z. Ajaltouni, S. Akar *et al.*, "Measurement of the electron reconstruction efficiency at lhcb," *Journal of Instrumentation*, vol. 14, no. 11, p. P11023, 2019.

[17] G. A. Cowan, D. C. Craik, and M. D. Needham, "Rapidsim: an application for the fast simulation of heavy-quark hadron decays," *Computer Physics Communications*, vol. 214, pp. 239–246, 2017.

[18] J. Beringer *et al.*, "Particle data group," *Phys. Rev. D*, vol. 86, no. 010001, 2012.